Materials & Design 223 (2022) 111121

Contents lists available at ScienceDirect

Materials & Design

journal homepage: www.elsevier.com/locate/matdes

Modelling and optimising hybrid process of wire arc additive manufacturing and high-pressure rolling

Valeriy Gornyakov, Yongle Sun *, Jialuo Ding, Stewart Williams

Welding and Additive Manufacturing Centre, School of Aerospace, Transport and Manufacturing, Cranfield University, Cranfield MK43 0AL, UK

HIGHLIGHTS

- Inter-layer, stacked-layers and post-build rolling is modelled to investigate their interaction with wire arc additive manufacturing (WAAM) for mitigating WAAM residual stress and distortion.
- Difference in mitigation efficacy of rolling using flat roller and slotted roller is demonstrated and explained.
- Influence depth of cyclic WAAM deposition and rolling to alter plastic strain that causes residual stress is determined and analysed for different process conditions.
- Hybrid process of WAAM and rolling can be optimised through changing the number of deposition layers for each rolling cycle and modifying the roller geometry.

GRAPHICAL ABSTRACT

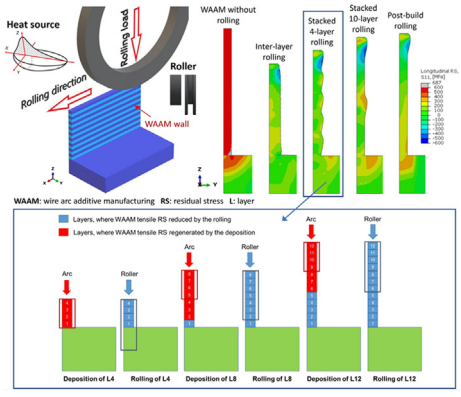

ARTICLE INFO

Article history:
Received 9 April 2022
Revised 15 August 2022
Accepted 4 September 2022
Available online 6 September 2022

Keywords:
Directed energy deposition
Cold working
Residual stress
Distortion
Numerical simulation

ABSTRACT

Hybrid process of wire arc additive manufacturing (WAAM) and high-pressure rolling can build large-scale components with low detrimental residual stress (RS) and distortion. We developed an efficient coupled process model for a steel wall to simulate the interaction between WAAM deposition and rolling. The predicted RS distributions and wall dimensions agree well with experimental results. Cyclic variation of longitudinal tensile RS occurs during WAAM deposition and inter-layer rolling in clamped condition. The influence depth of deposition and rolling is characterised by the number of the underlying layers that are plastically deformed after each process cycle. For the inter-layer rolling with a flat roller, the rolling has smaller influence depth than the deposition; consequently, the rolling does not eliminate but rather contains the regeneration of WAAM tensile RS after thermal cycles. Rolling with a slotted roller introduces more tensile plastic strain and thereby more effectively reduces WAAM tensile RS and unclamping distortion. Compared to the inter-layer rolling, stacked-four-layer rolling has larger influence depth and hence achieves similar RS mitigation efficacy with fewer rolling operations, while post-build rolling has lower efficacy due to insufficient penetration. Therefore, stacked-layers rolling with slotted roller is recommended for an optimal hybrid process of WAAM and rolling.

* Corresponding author.
E-mail address: yongle.sun@cranfield.ac.uk (Y. Sun).

https://doi.org/10.1016/j.matdes.2022.111121
0264-1275/

1. Introduction

Wire arc additive manufacturing (WAAM) is emerging as a new directed energy deposition process for small batch near-net-shape production of medium-/large-scale components in aerospace, automotive, energy and other industries [1–4]. WAAM relies on sequential deposition of metal layers in an open environment or a controlled chamber using a wire consumable as the feedstock, an electric arc as the heat source shielded with inert gas, and a robotic arm or gantry machine as the manipulator under precise control by a computer system. A wide variety of wire materials are available in the market for WAAM deposition, such as steels [5,6], aluminium alloys [7,8], titanium alloys [9,10], nickel superalloys [11,12] and functionally graded materials [13,14]. WAAM is well suited for industrial applications thanks to its high deposition rate, reduced manufacturing time, enhanced design flexibility, decreased buy-to-fly ratio and low build-up and operational cost [4,9,15,16].

The arc heat source utilised in WAAM causes local heating and uneven thermal expansion in the deposit and its surrounding material. Consequently, local plastic deformation occurs as the material is susceptible to yielding at high temperatures. In the subsequent cooling, the deposited hot material tends to shrink, but the surrounding material constrains the thermal shrinkage. The mismatch between the process-induced permanent deformations that are accumulated in different regions gives rise to residual stress (RS) [17]. RS and distortion are the main technical challenges facing WAAM for its wider adoption in industry [4,5]. The RS can cause cracks and degradation of fatigue performance, induce brittle fracture and reduce corrosion resistance [18–21], whilst excessive distortion can make the WAAM process unstable and the component unsuitable for assembly or service.

Several techniques have been proposed to mitigate WAAM-induced RS and distortion, such as rolling [5], in-situ induction heating [22,23] and post-build heat treatment [24]. The development of optimal tool path could also reduce RS and distortion in WAAM [25].

High-pressure rolling has been extensively studied in experiments for mitigating RS and distortion in WAAM. Colegrove et al. [5] applied rolling in steel WAAM components using both profiled roller (i.e., roller with concave contact surface) and slotted roller. They investigated several rolling strategies, including inter-layer rolling, rolling every four deposited layers (i.e., stacked-four-layer rolling) and rolling only on the last deposited layer (i.e., post-build rolling). According to their measurements after removal of clamps, the slotted roller was more effective than the profiled roller to reduce the peak tensile RS and the bending distortion. Martina et al. [26] reported a similar reduction of RS and distortion in inter-layer rolled Ti-6Al-4V WAAM components. Hönnige et al. [27] evaluated the inter-layer rolling using convex-shaped roller in Ti-6Al-4V WAAM intersections. They found that the RS distribution in the intersection was hardly affected by the rolling, presumably because the thermal deposition cycle had a stronger influence than the rolling on the final distribution of RS.

Despite the demonstrated effectiveness of rolling to reduce RS and distortion, the inter-layer rolling for WAAM still faces several practical challenges. For instance, in previous experiments, the rolling commenced only when the deposit cooled below 50 °C, and the rolling on each layer took remarkable time [5]. In addition, the slotted roller required application of lubricant before rolling of each layer, followed by degreasing [5]. All these operations significantly increased the manufacturing time and energy consumption. Process optimisation is hence needed to improve manufacturing efficiency, which requires a thorough understanding of the mechanism governing the RS and distortion.

The finite element method (FEM) was successfully applied in the simulation of rolling [28,29], which helped obtain detailed information to understand the rolling effect. Despite the recent research on modelling of post-build rolling for WAAM components, the simulation of inter-layer rolling that is applied throughout the WAAM deposition process has not been reported in the literature. One main challenge faced here is the high computational cost of a rolling model coupled with WAAM deposition. For example, it took about 95 h to obtain the solution of a single-pass rolling simulation for a 456 mm long welded component [30]. To tackle the computational challenge, Gornyakov et al. [31,32] recently developed an efficient modelling approach based on reduced-length model and steady-state solution mapping technique, which is applicable to both WAAM and rolling.

The recent modelling research on post-build rolling has shed some light on the influences of different parameters on the rolling efficacy to mitigate the RS and distortion in WAAM built walls. Gornyakov et al. [33] investigated the formation of plastic strain (PS) and RS in both unrolled and rolled states for a WAAM deposited wall, and elucidated the mechanism responsible for the mitigation of RS and distortion. Abbaszadeh et al. [34] and Tangestani et al. [35] studied the effects of the roller shape, rolling load and other parameters on distributions of RS and PS. For in-process rolling, it is anticipated that more complicated cyclic PS and RS formation occurs due to the alternate WAAM deposition and rolling.

The present study is aimed to reveal the complex interaction between WAAM deposition and rolling and thereby optimise the rolling strategy for the hybrid process to mitigate RS and distortion of WAAM component. An efficient finite element model is developed for the coupled process simulation, and to the authors' best knowledge, this is the first attempt to model and understand the complicated in-process rolling during WAAM deposition, while post-build rolling simulations have been already attempted by the authors [32,33] and other researchers [34,35]. Different roller shapes and rolling strategies are examined and evaluated to improve the efficacy and efficiency of the rolling for a WAAM built component.

2. Material and methods

2.1. Experiment

The WAAM component studied here was deposited and inter-layer rolled in a previous experiment [5]. Twenty layers with dimensions of approximately 490 mm × 5 mm × 2 mm for each layer were deposited to build a steel wall using a Cold Metal Transfer (CMT) process with a wire speed of 10 m/min (0.8 mm diameter G3Si1/ER70S-6 wire) and a torch travel speed of 500 mm/min. The CMT process offered high deposition rate and low heat input, which are beneficial for enhancing productivity and thermal control. The process parameters were selected based on experimental trials to achieve the target layer width and height. The used S355JR-AR grade steel substrate plate was 500 mm long, 60 mm wide and 12 mm thick, and restrained with six clamps during the WAAM deposition and rolling. The inter-layer rolling was conducted by controlling the vertical load (i.e., rolling load) on the pivot of the roller and moving the roller without application of torque. The sketch of the equipment and configuration for the WAAM and rolling, as well as the clamps locations, are presented in Fig. 1. Similar experimental setup for different materials can be also found in Refs. [27,36].

Both profiled and slotted rollers were used in the experiment, and the inter-layer rolling commenced when the deposit cooled down to 50 °C. For the slotted roller, the rolling was not started until the deposited wall reached a height larger than the depth (i.e., 10 mm) of the slot of the roller. A lubricant was applied to

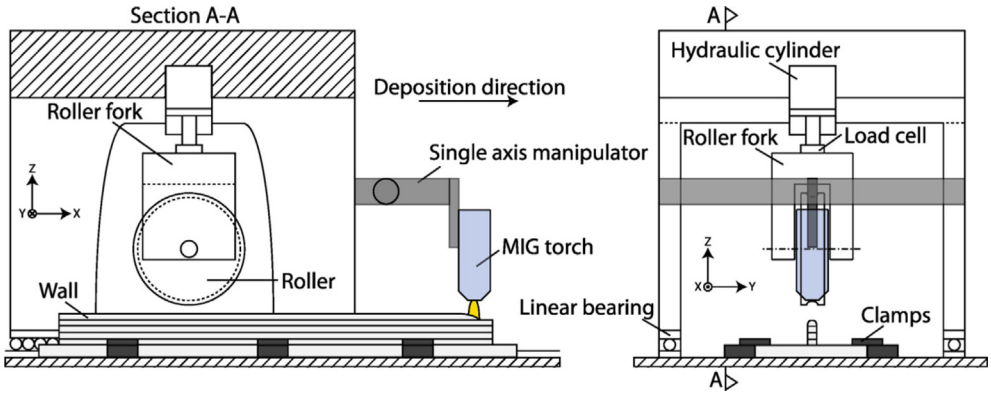

Fig. 1. The sketch of experimental equipment and setup for WAAM deposition and rolling [5].

the deposited wall before each run of rolling with the slotted roller, which was then degreased before depositing the subsequent layer. The neutron diffraction method was employed to measure the RS after the clamps were removed from the substrate. The out-of-plane distortion along the bottom line of the substrate after unclamping was measured using vernier callipers and a laser scanner. Details of the experiment can be found in Ref. [5].

2.2. Reduced-length thermal model of WAAM deposition

A short thermal multi-layer model was generated to obtain the temperature field in the steady-state region during WAAM deposition [32] (Fig. 2). To improve computational efficiency the component length was reduced to 72 mm in the model. The adopted length ensures that the WAAM model reaches steady-state and predicts a temperature field consistent with the full-length thermal model [32]. Double ellipsoidal heat source model [37] was employed, i.e.,

$$q_f = \frac{6\sqrt{3}f_f Q}{\pi\sqrt{\pi}a_f bc} e^{\left[-3\left(\frac{(x-vt)^2}{a_f^2}+\frac{y^2}{b^2}+\frac{z^2}{c^2}\right)\right]} \quad (1)$$

$$q_r = \frac{6\sqrt{3}f_r Q}{\pi\sqrt{\pi}a_r bc} e^{\left[-3\left(\frac{(x-vt)^2}{a_r^2}+\frac{y^2}{b^2}+\frac{z^2}{c^2}\right)\right]} \quad (2)$$

where q_f and q_r are the power density in the front and rear regions, respectively; f_f and f_r are the front and rear power distributing factors, respectively; Q is the net power input (arc efficiency is considered); v is the travel speed of the heat source and t is the travel time; a_f and a_r indicate the lengths of the front and rear regions, respectively; and b and c denote the lateral and vertical radii of the heat source, respectively. The heat source parameters were adopted from Ref. [38], i.e., $f_f = 0.6$, $f_r = 1.4$, $Q = 2245.83$ W, $a_f = 2$ mm, $a_r = 6$ mm, $b = 2.5$ mm and $c = 3$ mm. The addition of material was simulated by sequential activation of the whole layer for each deposition.

The thermal model is same as that reported in Ref. [32], which shows good agreement between predictions and thermocouple measurements of temperature histories at four locations. However, the mechanical model for present study is different from that in Ref. [32], see Section 2.3.

2.3. Reduced-length mechanical model of WAAM deposition and rolling

2.3.1. Overview of mechanical model

Fig. 3 presents the short mechanical model of multi-layer deposition and rolling for the clamped WAAM wall with a reduced length of 72 mm. As demonstrated in Ref. [32], the reduced-

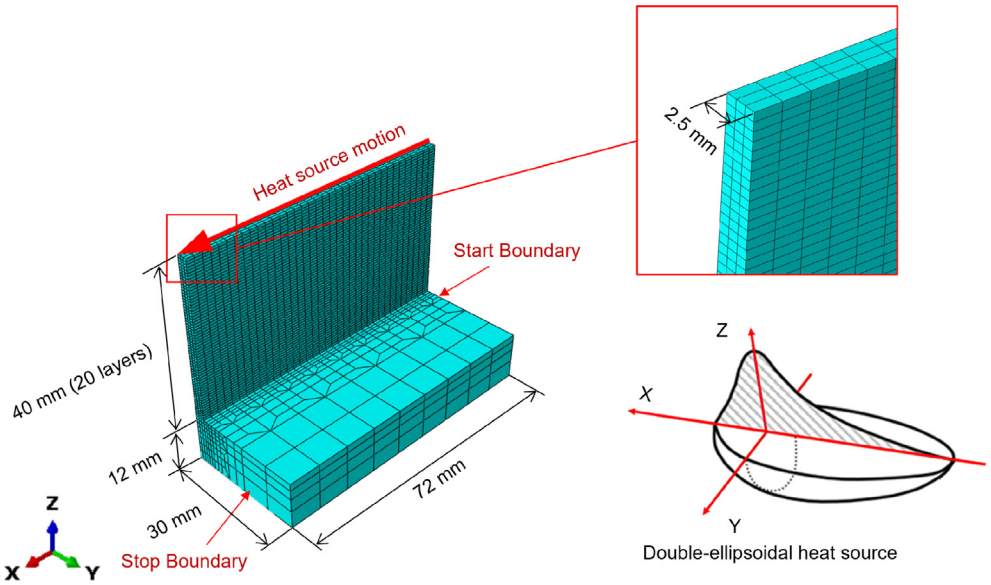

Fig. 2. Reduced-length multi-layer thermal model for the WAAM process (only half part is modelled due to symmetry).

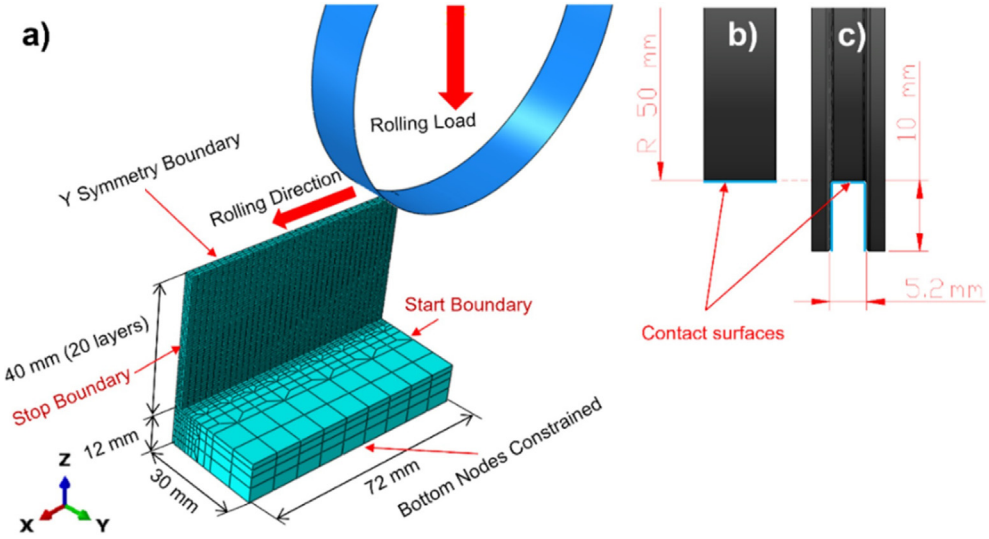

Fig. 3. (a) Reduced-length mechanical model for multi-layer WAAM deposition and rolling (only half part is modelled due to symmetry); (b) and (c) show the geometry of the flat and slotted rollers, respectively (contact surfaces are highlighted in blue). (For interpretation of the references to colour in this figure legend, the reader is referred to the web version of this article.)

length mechanical model did not sacrifice the fidelity of the steady-state solution but significantly saved computational time. The adopted length is sufficient for both WAAM and rolling to reach the steady state. During WAAM simulation, all nodes were constrained in the longitudinal direction to counteract the effect due to the reduction in component length [32], while the longitudinal constraint was relaxed except on the two end surfaces during the rolling simulation [32]. A simplified clamping constraint was implemented, i.e., the movement of all nodes on the bottom surface of the substrate were constrained in all directions. In addition, the layer surface was assumed to be flat which is commonly accepted for WAAM and rolling simulations [32,33,38]. Such geometric simplification circumvented element distortion potentially occurring during the hybrid process and it also significantly enhanced model convergence rate without sacrificing the key physics examined. As post-build rolling was already simulated in Refs. [32,33], the present study is focused on modelling of the interaction between WAAM deposition and rolling during the building process.

Abaqus FEM software package was used for the numerical simulations. The mechanical model was meshed using 9036 hexahedral linear elements with reduced integration, and the mesh topology was same as in the thermal model. The element dimensions vary from being small in the wall (2 mm $\times$ 0.833 mm $\times$ 0.667 mm) to being large in the substrate (8 mm $\times$ 7.5 mm $\times$ 1.765 mm). A sensitivity analysis showed that an increase in the mesh density did not affect the solution. It should be noted that the mechanical model and the thermal model were generated separately, while the temperature field predicted by the thermal model was imported into the mechanical model for subsequent analysis.

2.3.2. Coupling between WAAM deposition and rolling

For the inter-layer rolling studied here, both uncoupled and coupled process models were developed and compared to examine the effects of process coupling on the prediction accuracy and thereby to evaluate the potential decoupling simplification for saving computational time. In terms of this research, the process coupling means that the mechanical variables for each layer of the rolling model is dependent on the mechanical solution of the WAAM model, and vice versa. By contrast, the thermal solution to the WAAM deposition was independent of the mechanical model. In the uncoupled process model, the mechanical solution of the short WAAM model was transferred to the short rolling model, using the steady-state solution mapping technique [32], but the rolling model solution was not incorporated in the WAAM model, and thus the mechanical solution of the WAAM model was independent of the rolling model. Both the uncoupled and coupled process models consist of the following simulation steps for each layer: new layer activation, WAAM deposition cycle, roller placement, roller compression, and rolling.

2.3.3. Roller shapes

The shapes of flat and slotted rollers are presented in Fig. 3b and c, respectively. The roller was simplified as an analytic rigid shell with a radius of 50 mm. For the given rolling load, the assumption of rigid roller does not affect the solution of both 2D [31] and 3D [34] models. The flat roller was used in the model for representing the profiled roller used in the experiment [5] to improve computational efficiency. Previous study [33] demonstrated that a flat roller model with a roller-to-wall friction coefficient $\geq$ 0.5 predicted RS and PS distributions similar to those predicted by a profiled roller model. In addition, the roller contact surfaces are simplified to be flat in the models (Fig. 3b and c), although in the experiments [5] the profiled and slotted rollers had curved surfaces. This simplification reduced the computational time. According to Abbaszadeh et al. [34] and Tangestani et al. [35], the variation of typical roller surface radius only minorly affected the rolling model solution (e.g., PS and RS).

2.3.4. Rolling parameters

During the rolling the indentation of the roller to the WAAM wall surface was simulated through controlling vertical displacement, which simplified the loading process and enhanced the numerical convergency. To reach the prescribed rolling load of 50 kN in the experiment, values of vertical displacement of the roller for each layer were found iteratively (note that only half rolling load was considered for the half part modeled, Fig. 3a). The roller was moved along the wall length with a speed of 3 mm/s, and only the rotation around the pivot was allowed. The flat roller only involves horizontal contact with the top surface of the wall (Fig. 3b), while the slotted roller has both horizontal and vertical contact surfaces (Fig. 3c). To simulate the unlubricated contact

between the flat roller and the wall a friction coefficient of 0.5 was specified. This value was also suggested by Cozzolino et al. [30] and Coules et al. [39]. A friction coefficient of 0.1 was used in the rolling model with the slotted roller for lubricated contact, which was also adopted in previous rolling simulations [40–42].

2.3.5. Material properties

Temperature-dependent material properties of S355 mild steel were adopted from the dataset reported by Thompson et al. [43]. The adopted elastic–plastic material properties include strain-hardening data for large deformation, and the difference between the wall deposit and the substrate was considered. The yield strength of the S355 mild steel, as suggested by Thompson et al. [43], is relatively low (390 MPa at room temperature), while according to the material certificate of the employed ER70-S6 wire [5], the minimum yield strength is greater than 502 MPa. In most cases the magnitude of WAAM tensile RS reached the yield strength of the material [44]. Colegrove et al. [5] measured a tensile longitudinal RS of 600 MPa at the border between the WAAM wall and the substrate. Therefore, to obtain more realistic simulation results, the yield strength of the modelled wall deposit was specified 50 MPa larger than the material data reported by Thompson et al. [43].

2.3.6. Categories of rolling model and strategy

The rolling models were divided into two sets (Table 1). The models in Set 1 were used for validation and investigation of PS and RS evolution during WAAM deposition and inter-layer (IL) rolling. The models in Set 2 were used for optimisation of the rolling strategy for the WAAM wall, which examine the stacked-layers (SL) and post-build (PB) rolling processes.

2.4. Full-length mechanical model for unclamping

The reduced-length mechanical model cannot predict the RS and distortion in the actual WAAM wall after the removal of clamps [32]. To overcome this limitation, the reduced-length model was solved in clamped condition and the obtained steady-state solution was transferred as initial condition to generate the full-length mechanical model. The full-length model has the identical mesh density, material properties and cross-sectional dimensions as the reduced-length model (Section 2.3), except the full length of 500 mm [5]. The full-length model also allowed consideration of the actual clamping locations and boundary conditions applied in the experiment [5], which has been demonstrated in Ref. [32]. The technique of steady-state solution mapping (see Ref. [32] for detail) was employed to transfer the mechanical variables from the reduced-length model of WAAM deposition and rolling to the full-length model for investigating the material response to the deactivation of clamping.

2.5. Computational efficiency

High performance computing facility was employed to solve the model for WAAM deposition and rolling. The reduced-length model with the flat roller took 8 h 37 min of wall clock time to complete the simulation using 16 CPUs, and the computational time was 14 h 35 min for the model with the slotted roller. Traditional rolling simulation for a 500 mm long WAAM wall could take 4 h 26 min for one layer, meaning that the simulation of 20-layer rolling would take over 88 h [31]. The simulation of WAAM deposition also takes significant time [38]. Therefore, it can be estimated that the reduced-length model of the WAAM deposition and IL rolling is at least 89% more efficient than the traditional full-length model. Moreover, the full-length mechanical model for simulating clamps removal (Section 2.4) is highly efficient, and the computational time was just 6 min 43 s using 2 CPUs.

2.6. Inspection plane and validation approach

The inspection plane in the short IL rolling model is assigned in the y-z plane, 48 mm away in the rolling direction from the start boundary. The model reached steady state in this region. For the long model the inspection plane is the mid-length plane of the wall. Longitudinal RS distributions were also obtained along the vertical path in the symmetry plane of the WAAM wall for the steady state.

To validate the IL rolling model, the predicted RS distributions and wall dimensions in the inspection plane were compared to experimental measurements by Colegrove et al. [5]. The magnitude of out-of-plane distortion was also compared between the prediction and the measurement [5].

3. Results

3.1. Key features of predicted residual stress and distortion

3.1.1. Predictions by reduced-length mechanical models

Fig. 4 shows contour maps of the predicted distributions of the longitudinal RS generated by the WAAM deposition alone and by the WAAM deposition + IL rolling with flat and slotted rollers. In the clamped condition, the deposition generated almost evenly distributed tensile RS in the wall. Compressive RS was formed in the major region of the substrate to balance the WAAM tensile RS. Most significant longitudinal RS was generated on the border between the wall and substrate. The IL rolling with the flat roller mitigated the tensile RS in the wall and the region underneath the wall/substrate border. A compressive RS region was formed 2 mm under the last rolled layer. The magnitude of tensile RS in the wall was substantially reduced by the IL rolling with the slot-

Table 1
Reduced-length mechanical models of multi-layer WAAM deposition and rolling.

	Roller shape	*Rolling strategy*	*Purpose*
Set 1	*Flat roller for uncoupled WAAM deposition and rolling model* * *Flat roller* *Slotted roller*	*Inter-layer (IL)*	*Model validation and process investigation*
Set 2	*Flat roller* *Slotted roller* *Flat roller* *Slotted roller* *Flat roller* *Slotted roller*	*Every 4 deposited layers – (Stacked 4L)* *Every 10 deposited layers – (Stacked 10L)* *Post-build – (PB)*	*Optimisation of rolling strategy*

* Except for this model, all other models are coupled between WAAM deposition and rolling.

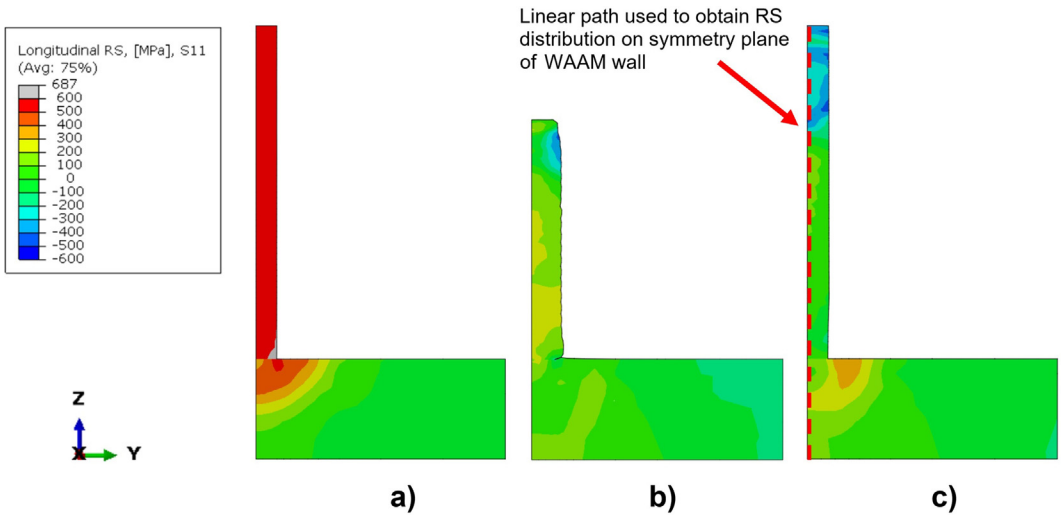

Fig. 4. Longitudinal RS distribution in WAAM deposited wall with clamps activated: (a) WAAM deposition only, (b) WAAM deposition + IL rolling using the flat roller, (c) WAAM deposition + IL rolling using the slotted roller.

ted rolled, and a more extensive region with compressive RS was generated under the rolled surface.

3.1.2. Predictions by full-length mechanical models

Figs. 5 and 6 show the 3D distributions of RS in the full-length component with clamps activated and deactivated, respectively, as obtained by the full-length mechanical models. A relaxation of tensile RS in the wall and a bending distortion (concave upwards) of the component (Fig. 5a and 6a) were caused by the deactivation of clamps in the model. Without clamping the magnitude of tensile RS reduced largely in the wall, as compared to the RS prediction with clamps activated. On the top of the wall, conversion of tensile RS to compressive RS occurred.

For the IL rolling with the flat roller, after the removal of clamps, the component slightly bended upwards, and the compressive RS underneath the rolled surface increased in magnitude (average value changed from −328 MPa to −494 MPa), as shown in Figs. 5b and 6b. In contrary, for the IL rolling with the slotted roller, the removal of clamps caused slight downward bending of the component. As a result, the magnitude of averaged compressive RS underneath the rolled surface reduced from − 470 MPa to − 370 MPa (Figs. 5c and 6c). The bending distortion along the bottom line of the substrate after removal of clamps is presented in Fig. 7, which clearly demonstrates the larger efficacy of the slotted roller to reduce the WAAM distortion.

3.2. Comparison with experimental results

The longitudinal RS distributions in the inspection plane after the removal of clamps were obtained by the full-length mechanical

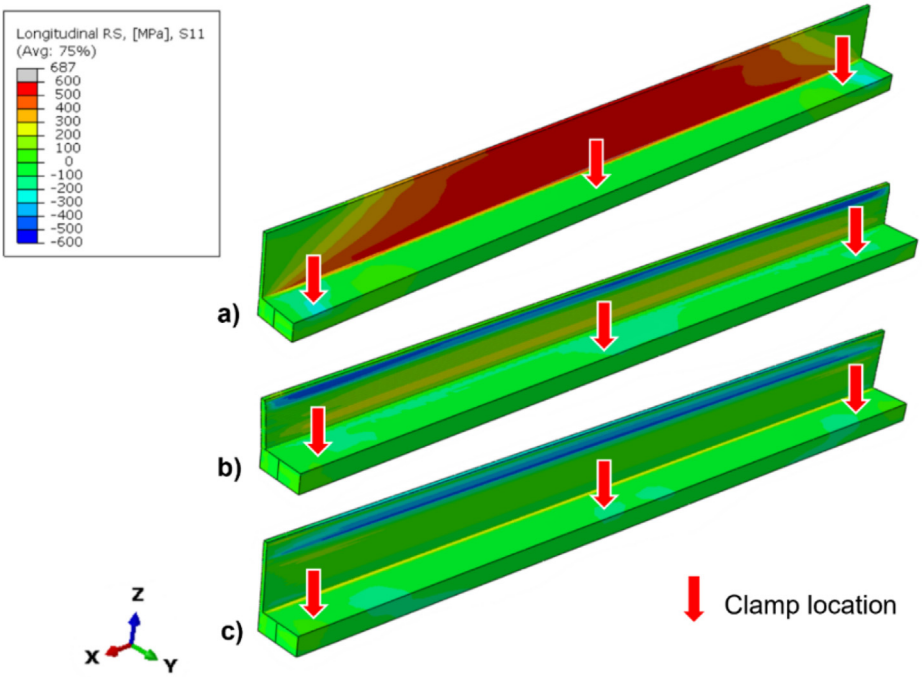

Fig. 5. Longitudinal RS distributions and deformed wall configurations before deactivation of clamps: (a) WAAM deposition only, (b) WAAM + IL rolling using the flat roller, (c) WAAM + IL rolling using the slotted roller (to aid visualisation a deformation scale factor of 5 is used).

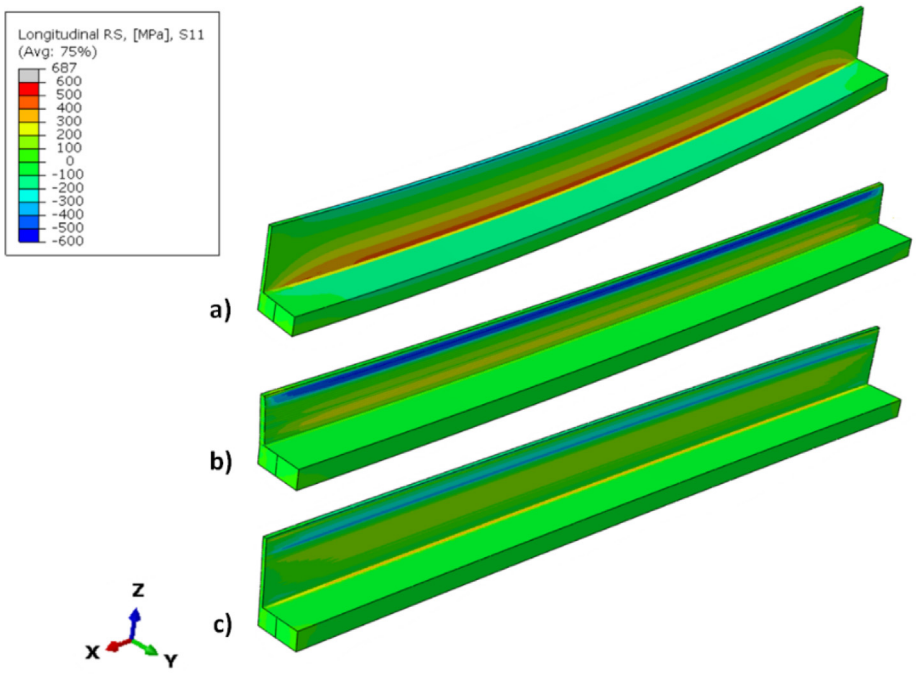

Fig. 6. Longitudinal RS distributions and deformed wall configurations after deactivation of clamps: (a) WAAM deposition only, (b) WAAM + IL rolling using the flat roller, (c) WAAM + IL rolling using the slotted roller (to aid visualisation a deformation scale factor of 5 is used).

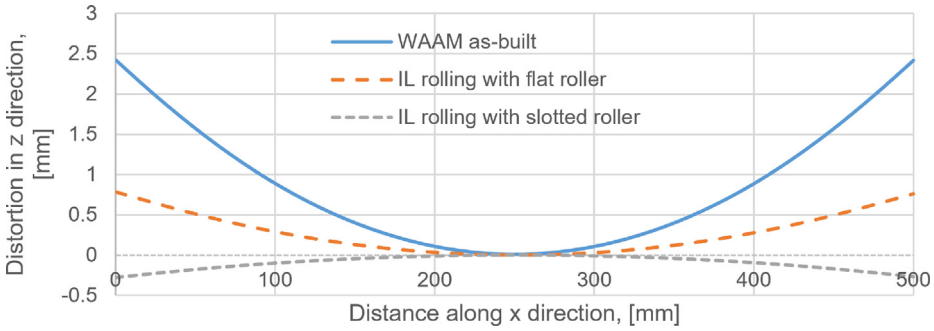

Fig. 7. Predicted distortion of the WAAM part after deactivation of clamps.

models with the flat roller, as shown in Fig. 8a. The steady-state solution in clamped condition was mapped from the coupled and uncoupled short WAAM + IL rolling models. The predictions are compared with experimental measurement [5]. The final RS distribution predicted by the coupled model overall matches well with the experimental measurement. The discrepancy is observed mainly in the region within a distance of 10 mm to the top of the wall. The full-length mechanical model associated with the uncoupled short model incorrectly predicted the final RS, as compared to the experimental data. This indicates that a process coupling model is necessary for the IL rolling simulation.

Fig. 8b shows the longitudinal RS distribution obtained by the full-length model associated with the coupled short model using the slotted roller, which is also compared to the experimental measurement [5]. The full-length model demonstrated a good correlation with the measurement in the region from 10 to 28 mm through the wall height. However, the model underpredicted RS in the wall closer to the substrate and predicted local peaks of compressive and tensile RS in the upper part of the wall, while such peaks were not observed in the experimental measurement [5].

The local discrepancy between the prediction and measurement (Fig. 8) could be partially attributed to the limitations of the neutron diffraction measurement technique [45]. It is well known that neutron diffraction measurement is sensitive to microstructure, and its resolution is limited to the gauge volume adopted. Martina et al. [26] measured the RS in the top layers of Ti-6Al-4V WAAM + IL rolled wall using the contour method, and they observed RS distribution trend similar to the one obtained from the present model. Given the complexity of the hybrid process, the prediction accuracy of the model is deemed sufficient for the purpose of this study.

Fig. 9 shows the deformed configurations of the rolled wall on the y-z inspection plane. The predictions of the width of the rolled wall by the reduced-length IL rolling models matched with the observations in the macrographs [5]. The discrepancy between the predicted and measured widths of the rolled wall is 2.7% and 0% for the rolling with the flat and slotted rollers, respectively. For the slotted roller, the rolled wall width is equal to the width of the slot (i.e., 5.2 mm, Fig. 3c).

The predictions for rolled wall height also agree well with the experiments [5]. For the flat roller model, the predicted height is 28.48 mm, while the measured height is 28.0 ± 0.2 mm. The IL rolling with the slotted roller barely changed the wall height compared to the as-built condition, which is consistent between the

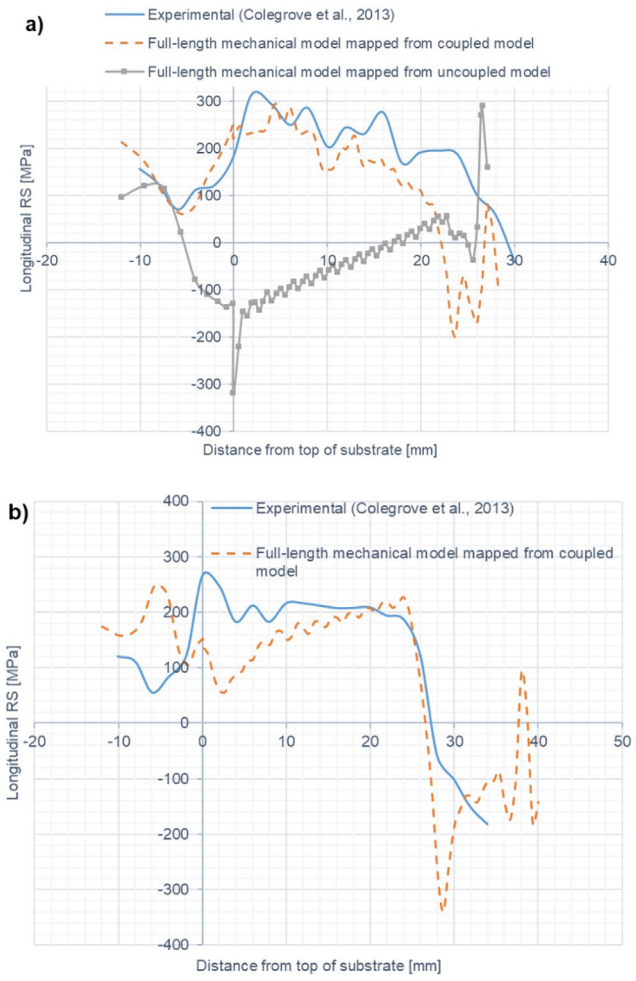

Fig. 8. Longitudinal RS distributions along the vertical path in the symmetry plane for the full-length mechanical models after clamps deactivation, compared to experimental measurements [5]. The flat roller (a) and slotted roller (b) were used in the rolling simulations, and the full-length model was based on the solution mapped from the steady-state region of the reduced-length WAAM + IL rolling model.

prediction and measurement. In the experiment [5], only the magnitude of the bending distortion was measured; hence, the experimental measurement is not included in Fig. 7. The model underpredicted the magnitude of the distortion. For instance, the maximum bending distortion in z-direction predicted by the model in the as-built condition is 2.4 mm, compared to 6.7 mm in the measurement [5]. The maximum distortion predicted by the WAAM + IL rolling model with the flat roller is 0.78 mm, while it is 2.6 mm measured experimentally. For the slotted roller, a downward distortion of −0.27 mm was predicted, while the experiment showed an upward distortion of 1.2 mm.

The underestimate of the distortion can be attributed to the limitations of the employed modelling method [32]. The rigid clamping through constraining all the nodal displacements on the substrate bottom is assumed in the short mechanical models. However, in the experimental setup by Colegrove et al. [5], six thin clamps were applied to small regions on the surfaces of the substrate, which are anticipated to exhibit considerable compliance due to the limited rigidity of the clamps. As a result, in-process distortion is expected to occur which cannot be captured by the short model under fully rigid clamping. The influence of the less rigid clamping system on final distortion was also discussed by Colegrove et al. [5].

Despite the discrepancy in the magnitude of the distortion, the IL rolling model correctly captured the trend observed in the experiment, i.e., the rolling reduced the WAAM distortion, and the slotted roller was more effective than the flat roller. More sophisticated modelling approach to capture the in-process distortion would be developed in future study.

3.3. Temperature, stress and PS evolution during WAAM deposition and inter-layer rolling

Figs. 10–12 show the concurrent evolution of temperature, longitudinal stress and PS in layer 6 during the WAAM deposition of layers 6–14, coupled with IL rolling using the flat roller. The layer 6 is selected for inspection since it is less susceptible to the influence by the substrate and thus representative for the WAAM wall. The inspected element for the aforementioned physical variables is located in the inspection plane (Section 2.6) and adjacent to the symmetry plane and the top surface of the layer 6. All these results were obtained from the reduced-length model in the clamped condition (Section 2.3).

It is clearly seen from Fig. 10 that tensile RS (550 MPa) formed in layer 6 after the deposition, accompanying the generation of compressive PS in the deposit. The subsequent rolling of layer 6 introduced tensile PS and compressive RS (− 72 MPa). Although the subsequent deposition of layers 7 and 8 regenerated the tensile RS, the accompanied rolling continued inducing tensile PS and mitigating the tensile RS. However, after the rolling of layer 9, the RS tended to increase (Fig. 11a), since the subsequent rolling did not further introduce tensile PS, i.e., the PS in layer 6 is constant during the subsequent rolling stage, as shown in Fig. 11b. When the peak

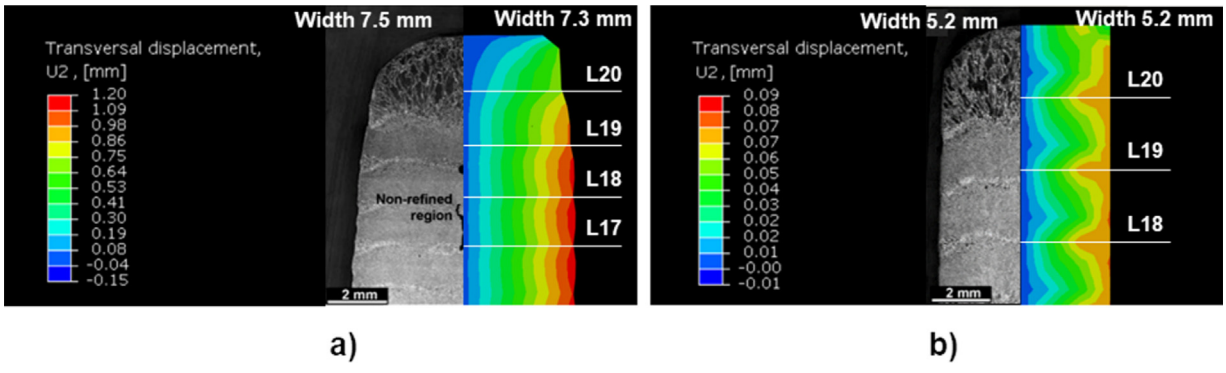

Fig. 9. Comparison of the predicted configurations of the rolled wall with experimental observations in macrographs [5]: (a) rolled with profiled roller in the experiment and flat roller in the simulation; (b) rolled with slotted roller in both experiment and simulation. The predicted wall width and transversal displacement after rolling are also shown.

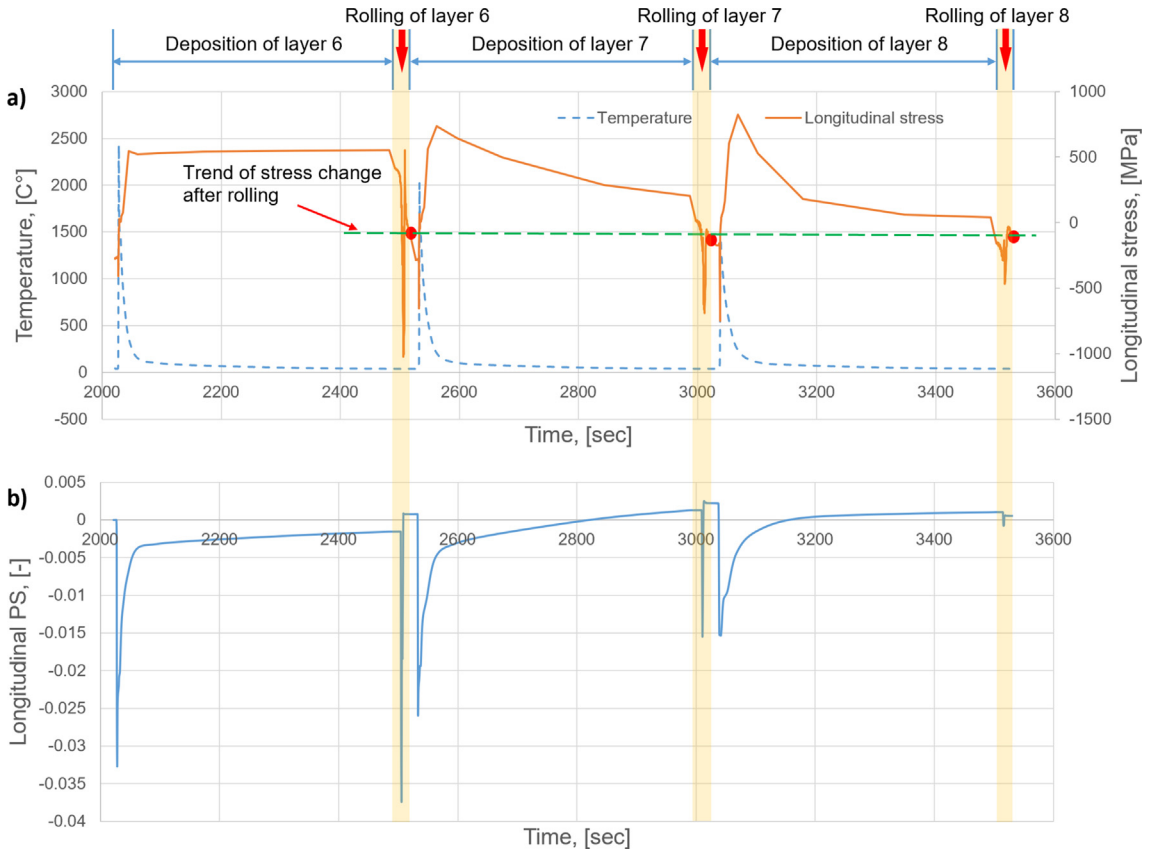

Fig. 10. Concurrent evolution of temperature and longitudinal stress (a), as well as the longitudinal PS (b), in the layer 6 during WAAM deposition of layers 6–8 in conjunction with IL rolling using the flat roller. The data were collected at the top of layer 6 in the inspection plane and the rolling phases are highlighted in the yellow shaded areas. (For interpretation of the references to colour in this figure legend, the reader is referred to the web version of this article.)

temperature in layer 6 dropped to 400 °C during deposition of layer 13 (Fig. 12a), the deposition also stopped generating PS in layer 6 (Fig. 12b). In other words, the subsequent alternation of deposition and rolling did not cause further plastic deformation in layer 6, and then the material response became fully elastic. Consequently, the RS was stabilised, and its magnitude was lower than that in a WAAM process without IL rolling. Thanks to the IL rolling with the flat roller, the initially formed WAAM tensile RS in layer 6, reduced from 550 MPa to 201 MPa after the rolling.

For the IL rolling with the slotted roller, the layer 9 was selected for inspection, since in such a case the rolling started from layer 6 to accommodate the depth of the slot (Fig. 3c), and the material response is more representative in the process cycles after layer 9. One element adjacent to the symmetry plan and the top surface was inspected to represent layer 9. Distinctive evolution of longitudinal PS and stress in layer 9 was found during the WAAM deposition of layers 9–16 in conjunction with IL rolling using the slotted roller (Fig. 13). Similar influence depth for generating PS was identified between the rolling and deposition. However, the deposition was unable to reverse the tensile PS induced by the rolling and hence there is accumulation of tensile PS during the evolution. Compared to the flat roller (Figs. 10–12), the slotted roller introduced higher tensile PS and thereby more effectively mitigated the WAAM-induced tensile RS (for layer 9 it reduced from 500 MPa to 3 MPa after deposition of layer 16).

3.4. Comparison between different rolling strategies

To examine the potential improvement of manufacturing efficiency through reducing runs of rolling, additional simulations were performed for cyclic rolling after WAAM deposition of several layers instead of each layer. Fig. 14 compares the predicted contour maps of longitudinal RS after the WAAM deposition only, and the WAAM plus IL, SL and PB rolling using the flat roller. These results were obtained from the inspection planes in the reduced-length mechanical models of WAAM deposition and rolling.

The stacked 4L rolling (Fig. 14c) led to RS distribution in the wall similar to the IL rolling (Fig. 14b), indicating the similar effectiveness for mitigating WAAM tensile RS (Fig. 14a). However, the stacked 10L rolling (Fig. 14d) generated local peaks of tensile RS near the top surface, in the middle of the wall and beneath the wall in the substrate, despite similar RS distribution in the other region as compared to the IL rolling. The PB rolling (Fig. 14e) only effectively reduced the WAAM tensile RS in the upper half of the wall. Compared with the IL and SL rolling strategies (Fig. 14b–d), the PB rolling was less effective to mitigate the WAAM tensile RS in the bottom part of the wall and in the substrate (Fig. 14e). It was also found that the more runs of rolling with the flat roller, the lower height of the rolled wall (Table 2).

Fig. 15 compares contour maps of the longitudinal RS in the inspection plane (Section 2.6) for WAAM without rolling, and WAAM with IL, SL and PB rolling when the slotted roller was used in the simulations. There is only a minor difference in RS distribution between the IL and stacked 4L rolled WAAM walls (Fig. 15b and c). The stacked 10L rolling generated RS distribution overall similar to the IL rolling, but it gave rise to a local peak of tensile RS (470 MPa) in the mid-height region of the wall. After the PB rolling, the wall region near the substrate remained being subjected to pronounced tensile RS (388 MPa). Nevertheless, the WAAM tensile RS was largely reduced by the rolling in most regions. The slotted roller was less effective to mitigate the WAAM tensile RS in the substrate, despite the larger induced compressive RS region in

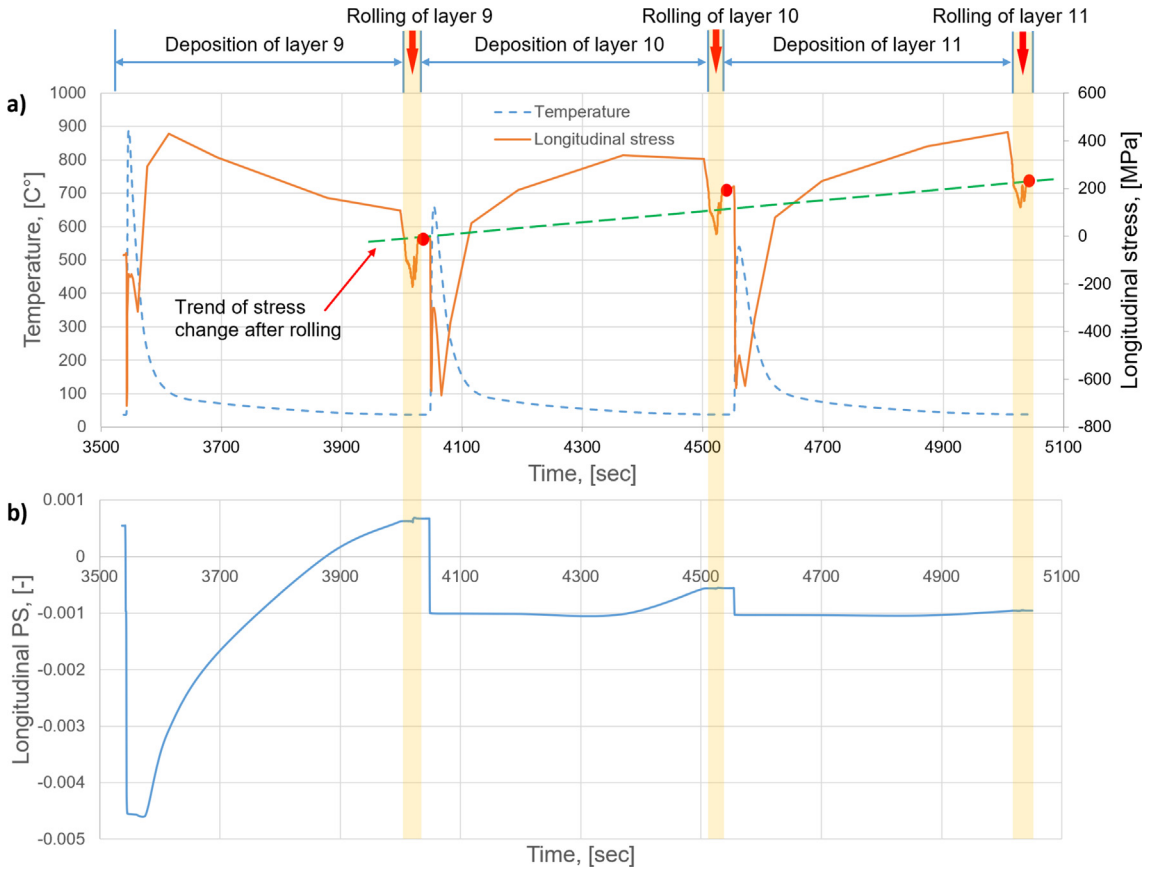

Fig. 11. Concurrent evolution of temperature and longitudinal stress (a), as well as longitudinal PS (b), in the layer 6 during WAAM deposition of layers 9–11 in conjunction with IL rolling using the flat roller. The data were collected at the top of layer 6 in the inspection plane and the rolling phases are highlighted in the yellow shaded areas. (For interpretation of the references to colour in this figure legend, the reader is referred to the web version of this article.)

the wall as compared to the flat roller (Figs. 14 and 15). This occurred because the slotted roller started rolling later than the flat roller due to the slot depth. The height of the rolled wall hardly changed with increasing the number of rolling runs (Table 3).

4. Discussion

4.1. Residual stress and distortion

4.1.1. Multi-layer deposition and rolling in clamped condition

The WAAM-induced longitudinal tensile RS was effectively mitigated by the IL rolling with the flat and slotted rollers at the 50 kN rolling load in the clamped condition (Fig. 4). The RS mitigation can be attributed to the rolling-induced change in PS distribution. Figs. 16 and 17 show the PS distributions generated by WAAM deposition, as well as WAAM with IL, SL and PB rolling using the flat and slotted rollers. The rolling introduced tensile PS, and overall reduced or eliminated the WAAM-induced compressive PS, despite some localised compressive PS bands remaining after rolling. As a result, the RS distributions changed after the applied different rolling strategies.

As shown in Figs. 14 and 15, the slotted roller, in comparison with the flat roller, led to larger compressive RS in the upper part of the WAAM wall and smaller tensile RS in the lower part of the wall, particularly pronounced for SL and IL rolling. This difference can be attributed to the ability of the slotted roller to induce larger tensile PS in the core of the wall (Figs. 16 and 17). The slot of the roller provides a lateral restraint effect on the wall, whereas the flat roller does not restrict the transversal displacement. Specifically for the simulations of the IL rolling, the flat roller increased the wall width by 2.3 mm, while the slotted roller led to widening only by 0.2 mm, as compared to the as-deposited wall (Figs. 2 and 9). The slotted roller eliminates transversal deformation under vertical compression and hence promotes longitudinal tensile PS during the rolling (Fig. 17). Consequently, the slotted roller is more effective to mitigate WAAM tensile stress (Figs. 14 and 15). This finding is consistent with the previous experimental observations for IL and SL rolling [5] and the numerical studies for PB rolling [33].

The RS distribution produced by the IL rolling with the slotted roller is more beneficial than that for the flat roller. The lower magnitude of the tensile RS in the clamped wall leads to lower bending distortion after removal of clamps (Fig. 7). The larger compressive RS in the upper region of the wall improves fatigue performance of the built component [46,47]. Furthermore, the slotted roller does not reduce the height of the rolled component (Table 3), avoiding material waste and additional layer deposition to achieve the designed height.

4.1.2. Deposited and rolled wall after removal of clamps

The IL rolling using the flat and slotted rollers reduced the bending distortion caused by the relief of WAAM tensile RS after removing clamps (Fig. 6). The distortion of the as-built component was driven by the large longitudinal tensile RS that was not completely self-balanced in the wall under the clamped condition, which created a net bending moment on the clamps. After removal of clamps, a pronounced redistribution of RS caused significant bending distortion (Fig. 6a). The IL rolling reduced tensile RS and induced compressive RS in the clamped wall. This change in RS

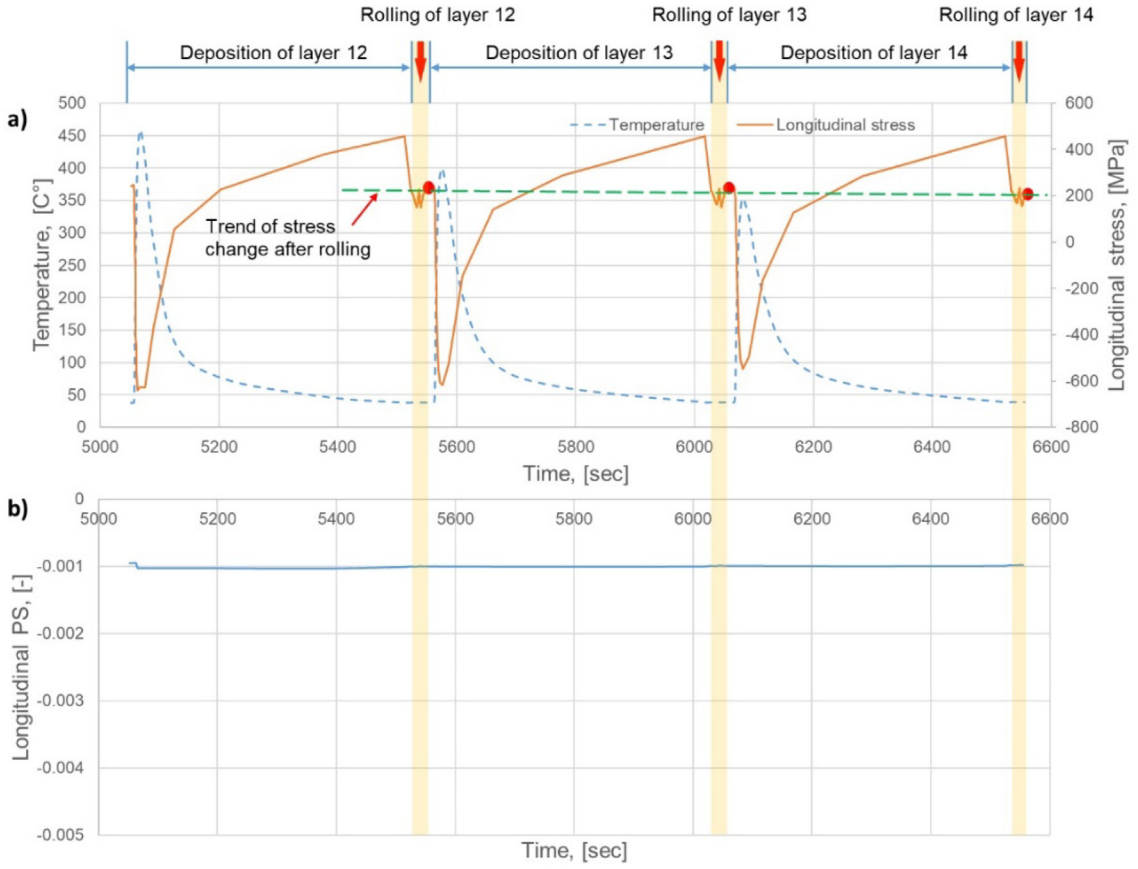

Fig. 12. Concurrent evolution of temperature and longitudinal stress (a), as well as longitudinal PS (b), in the layer 6 during WAAM deposition of layers 12–14 in conjunction with IL rolling using the flat roller. The data were collected at the top of layer 6 in the inspection plane and the rolling phases are highlighted in the yellow shaded areas. (For interpretation of the references to colour in this figure legend, the reader is referred to the web version of this article.)

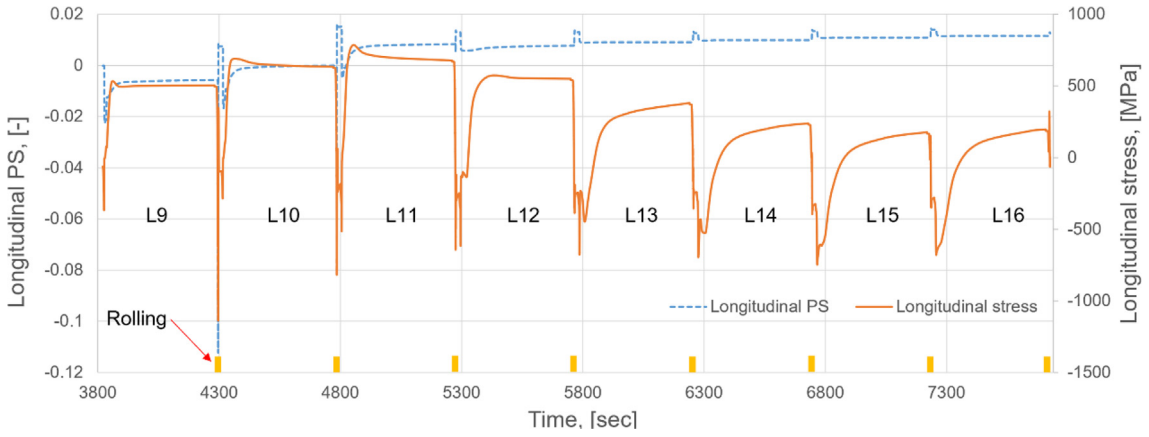

Fig. 13. Concurrent evolution of the longitudinal PS and stress in the layer 9 during WAAM deposition of layers 9–16 in conjunction with IL rolling using the slotted roller. The data were collected at the top of layer 9 in the inspection plane (the slotted roller started rolling on layer 6), and the rolling phases are highlighted in the yellow shaded areas. (For interpretation of the references to colour in this figure legend, the reader is referred to the web version of this article.)

state markedly reduced the net bending moment exerted on the clamps. Indeed, much lower nodal forces at the clamping points were predicted by the WAAM + rolling model, as compared to the WAAM model without rolling [32,33]. The RS state in the IL rolled component was close to complete self-balance and a new equilibrium was reached shortly after unclamping. A minor redistribution of RS occurred, resulting in relatively small distortion (Figs. 6b and c, and 7).

Interestingly, the IL rolling using the slotted roller caused the WAAM component to slightly bend in the opposite direction compared to the IL rolling with the flat roller (Figs. 6 and 7). As the slotted roller induced tensile PS of larger magnitude in a larger volume of the wall (Figs. 16b and 17b), the tensile RS in the upper region of the wall converted to compressive RS (Figs. 4c and 5c). Consequently, after removing clamps, compressive RS partially relieved and caused the component to slightly bend downwards (Figs. 6c and 7).

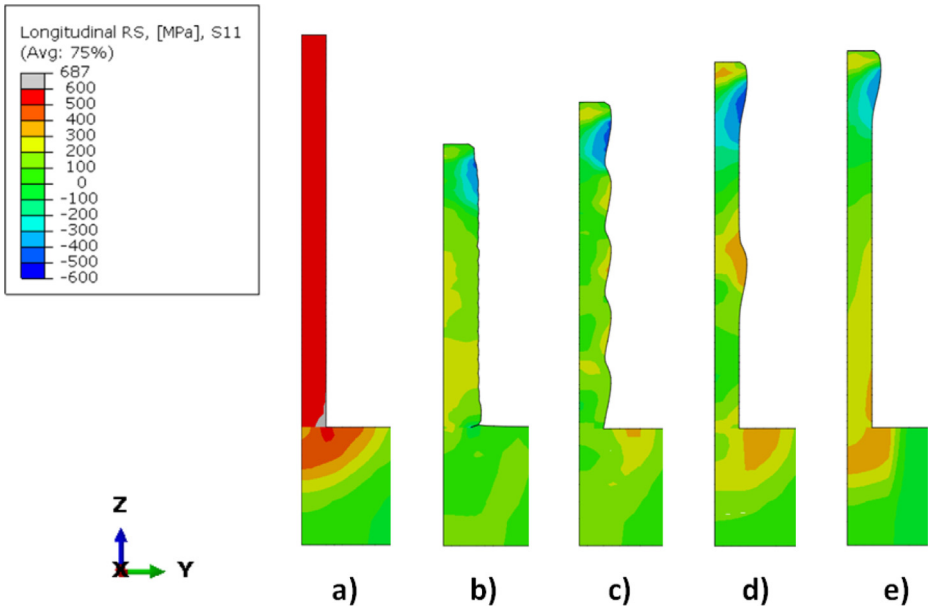

Fig. 14. Longitudinal RS contour maps in clamped condition: (a) WAAM deposition only, (b) WAAM deposition + IL rolling, (c) WAAM deposition + stacked 4L rolling, (d) WAAM deposition + stacked 10L rolling, (e) WAAM deposition + PB rolling. The flat roller was used in the rolling simulations.

Table 2
Wall height after WAAM + rolling with the flat roller.

Rolling strategy	WAAM without rolling	WAAM + IL	WAAM + stacked 4L	WAAM + stacked 10L	WAAM + PB
Rolling runs	0	20	5	2	1
Height of the wall [mm]	40	28.48	33.49	37.36	38.36

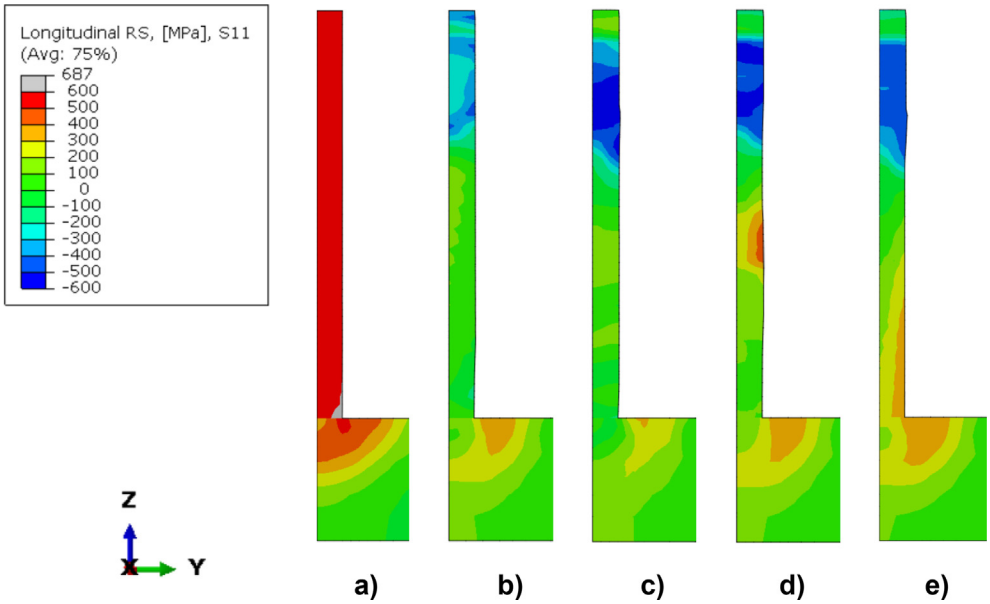

Fig. 15. Longitudinal RS contour maps in clamped condition: (a) WAAM deposition only, (b) WAAM deposition + IL rolling, (c) WAAM deposition + stacked 4L rolling, (d) WAAM deposition + stacked 10L rolling, (e) WAAM deposition + PB rolling. The slotted roller was used in the rolling simulations.

Table 3
Wall height after WAAM + rolling with the slotted roller.

Rolling strategy	WAAM without rolling	WAAM + IL	WAAM + stacked 4L	WAAM + stacked 10L	WAAM + PB
Rolling runs	0	20	5	2	1
Height of the wall [mm]	40	39.84	39.64	39.32	39.63

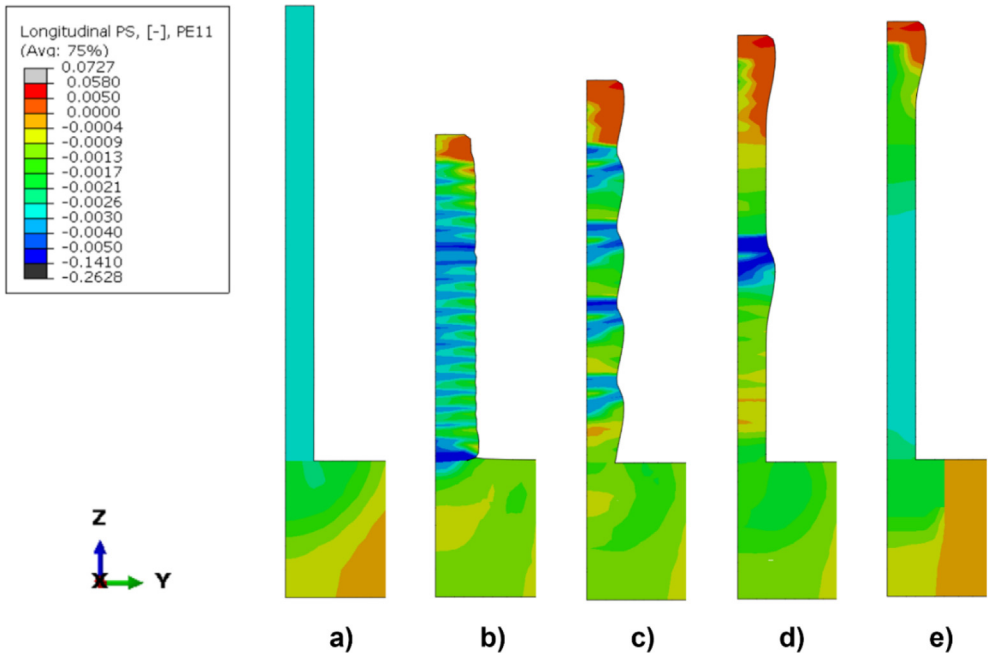

Fig. 16. Longitudinal PS contour maps in clamped condition: (a) WAAM deposition only, (b) WAAM deposition + IL rolling, (c) WAAM deposition + stacked 4L rolling, (d) WAAM deposition + stacked 10L rolling, (e) WAAM deposition + PB rolling. The flat roller was used in the rolling simulations.

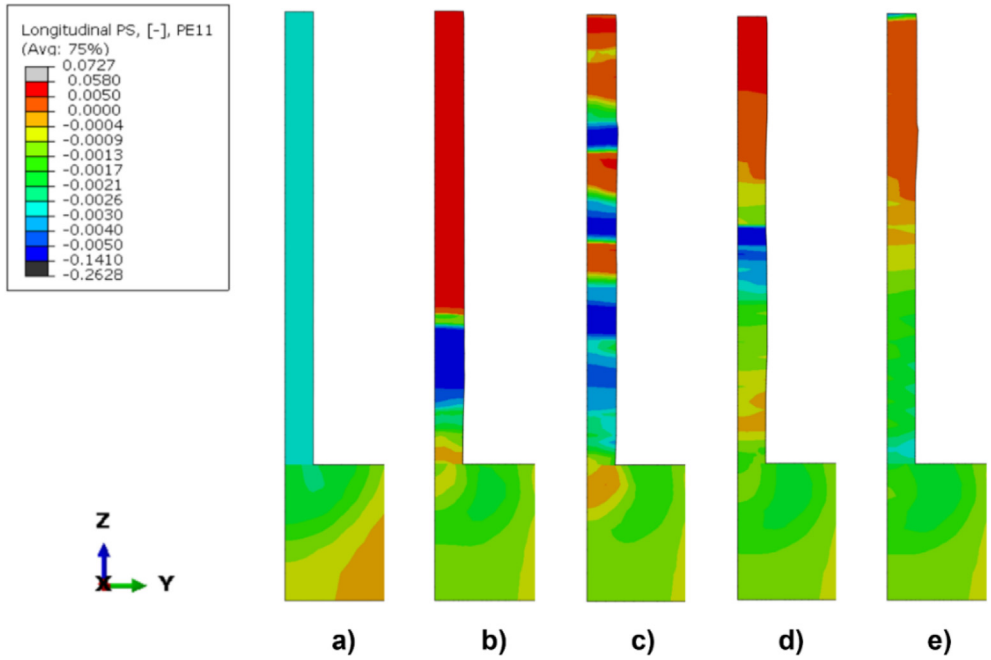

Fig. 17. Longitudinal PS contour maps in clamped condition: (a) WAAM deposition only, (b) WAAM deposition + IL rolling, (c) WAAM deposition + stacked 4L rolling, (d) WAAM deposition + stacked 10L rolling, (e) WAAM deposition + PB rolling. The slotted roller was used in the rolling simulations.

4.2. Deformation mechanism during WAAM + inter-layer rolling

In the hybrid process model, both the initial and final temperatures are room temperature. Therefore, the net thermal deformation of the modelled material is zero and the plastic deformation is the cause of the predicted RS. It should be noted that in this study the rolling was performed when temperature dropped below 50 °C. Although the rolling at high temperature is effective to modify the microstructure [48], the RS mitigation requires rolling temperature is low enough to avoid the potential RS build-up due to the cooling after rolling [49]. The rolling-enabled microstructural modification is another interesting topic and the thermal-mechanical model could be coupled with a metallurgical model to optimise the hybrid process for microstructural control in future study.

The evolution of PS demonstrates that the deposition and rolling of each layer have a certain depth of influence, i.e., the plastic deformation in the layers underneath the top surface was changed by the deposition or rolling, and the influence depth can be indicated by the number of the plastically deformed underlying layers.

In the layer 6, compressive PS was generated by the deposition of layers 6–12 (Figs. 10–12). However, during the deposition of layer 13 and subsequent layers, the peak temperature became insufficient (400 °C and lower) to initiate plastic flow in layer 6 (Fig. 12). The distance over 7 layers (i.e., layers 6–12) is thus considered as the depth of deposition influence for cyclic plasticity, below which the material solely undergoes elastic deformation during reheating and cooling (Fig. 12).

The tensile PS, as induced by the rolling, counteracted the WAAM-induced compressive PS in the rolled wall [33]. For the IL rolling with the flat roller, the rolling-induced PS in layer 6 reduced after new layers were deposited. The rolling after deposition of layer 10 virtually did not change the PS in layer 6 (Fig. 11), meaning that only 4 layers below the rolled surface were yielded by the rolling (Figs. 10 and 11). Therefore, the influence depth is 4 layers for the IL rolling with the flat roller.

As the deposition penetrates deeper than the rolling with the flat roller, the effectiveness of IL rolling to alter the RS induced by WAAM is limited. Nevertheless, the WAAM-induced compressive PS was overall lowered by the rolling (Fig. 16b), which has significant implication in RS development (Fig. 14). For instance, the rolling on the newly deposited layer 6 induced tensile PS and the WAAM tensile RS converted to compressive RS (Fig. 10). However, during deposition of subsequent layers, the regeneration of tensile RS in layer 6 occurred due to WAAM-induced thermal cycles, and the new tensile RS gradually increased after the rolling stopped further introducing PS (Fig. 11). The stress level in the layer 6 stabilised after the PS did not change anymore (Fig. 12). Considering the whole hybrid process, the IL rolling reduced WAAM tensile RS and contained its regeneration. As a result, the final longitudinal RS in the layer 6 reduced from 550 MPa to 201 MPa (Figs. 10–12).

The IL rolling with the slotted roller demonstrated twice the influence depth than the rolling with the flat roller, and it introduced a higher tensile PS (Fig. 13). This difference arises because the slotted roller imposes restraint in transversal deformation and promotes longitudinal plastic deformation (Fig. 17b). Although in such a case the deposition and rolling had the same influence depth, the rolling led to a greater change in PS. It is thus unsurprising that the longitudinal RS in the inspected layer was largely mitigated by the IL rolling with the slotted roller.

4.3. Optimisation of rolling strategy for hybrid process

The RS profiles produced by the stacked 4L rolling with the flat and slotted rollers are similar to the IL rolling (Figs. 14 and 15). Although no additional RS measurement is available to directly verify this, similar reduction in bending distortion after unclamping for both IL rolling and stacked 4L rolling was observed in experiments [5], suggesting similar RS before unclamping. Such similarity is probably associated with the increased influence depth for the SL rolling compared to the IL rolling.

The evolution of the longitudinal PS in layer 6 during WAAM deposition and stacked 4L rolling using the flat roller is shown in Fig. 18. The PS was influenced with a depth of 7 layers below the rolled surface for the stacked 4L rolling, while for the IL rolling only 4 underlying layers were influenced. On the other hand, the influence depth of deposition was 4 layers for the stacked 4L rolling (Fig. 18), compared to 7 layers for the IL rolling (Fig. 12).

The IL rolling penetration was resisted by the strain hardened material in the previously deposited and rolled layers. The increase in the width of the rolled wall also enhanced the rolling resistance (Fig. 14b). By contrast, during the stacked 4L rolling, deeper penetration was achieved at the identical rolling load due to the less strain hardening caused by the fewer rolling runs and less increase in the rolled wall width. As a result, the stacked 4L rolling has greater influence depth than the IL rolling. Regarding the WAAM influence depth, the less reduction in wall height during stacked 4L rolling could contribute to the reduced number of the underlying layers affected by the deposition, as compared to the IL rolling.

The above analysis explains the differences in influence depth between IL rolling and Stacked 4L rolling. However, it is challenging to quantify the individual contributions of mechanical and geometrical factors to such differences. Particularly for strain hardening, material can be softened by the reheating during subsequent deposition. The hardening history in the plasticity model can be eliminated at temperatures above a critical value. To accurately capture the influence depth of such material softening, the thermal model should be coupled with the mechanical model, such that the effect of the layer height reduction and width increase by rolling with the flat roller can be accounted for in the heat transfer analysis. This is still an open topic for future research.

Fig. 19 illustrates the mechanism of the cyclic variation of longitudinal RS during WAAM + stacked 4L rolling with the flat roller. Initially, WAAM deposition generated tensile RS in layers 1–4. As the rolling influence depth was 7 layers, the rolling on layer 4 mitigated the longitudinal tensile RS in the layers 1–4 and the substrate underneath the wall. As the deposition influence depth was 4 layers, the deposition of layers 5–8 caused new formation and reformation of tensile RS in layers 2–8. Subsequent rolling on layer 8 reduced tensile RS within 7-layer depth, i.e., in layers 2–8. Similar variation of RS occurred during deposition of layers 9–12 and rolling on layer 12. After the final rolling on layer 20, tensile RS in all layers was reduced by the stacked 4L rolling, which explains the RS distributions shown in Fig. 14c. The interaction between the rolling with the slotted roller and the deposition is also responsible for the RS evolution in the wall, but the RS distribution is distinctive due to the difference in the specific interaction involved.

The stacked 10L rolling using both rollers demonstrated a local peak of tensile RS in the mid-height region of the wall (Figs. 14d and 15d). This is because the rolling of two layers only (layer 10 and layer 20) was insufficient to reduce the compressive PS in the whole wall and high compressive PS was concentrated in the mid-height location (Fig. 16d and 17d). Similarly, a large tensile RS region close to the substrate was observed in the PB rolled wall (Figs. 14e and 15e). In such a case, solely rolling the last layer was inadequate to influence the whole wall (Figs. 16e and 17e) and extensive tensile RS remained.

The SL and PB rolling with flat and slotted rollers have the prospect to improve manufacturing efficiency by reducing the number of rolling operations. However, the WAAM component with stacked 10L rolling and PB rolling is not recommended for fatigue sensitive applications. The high tensile RS remaining in the wall can adversely affect the service life of the component [46,47]. Nevertheless, the PB rolling can efficiently mitigate RS and distortion in low height WAAM components [33].

Despite the longer manufacturing time required for removing the lubricant during the in-process rolling with the slotted roller, the use of the slotted roller reduced tensile RS in the whole wall to a greater degree and achieved lower distortion, as compared to the flat roller.

Another consideration for the evaluation of the hybrid process is the change of WAAM component dimensions after rolling, which also influences manufacturing efficiency. Larger reduction in wall height requires more deposited layers to achieve the designed height, and significant increase in wall width implies more extensive machining needed. Rolling with the slotted roller is preferential in this aspect since it caused negligible change in the wall height and width (Table 3 and Fig. 9b), while rolling with the flat roller caused more marked dimensional change (Table 2 and Fig. 9a). In addition, the reduced wall surface roughness of the components built with the slotted roller (Fig. 15) minimises post-build machining.

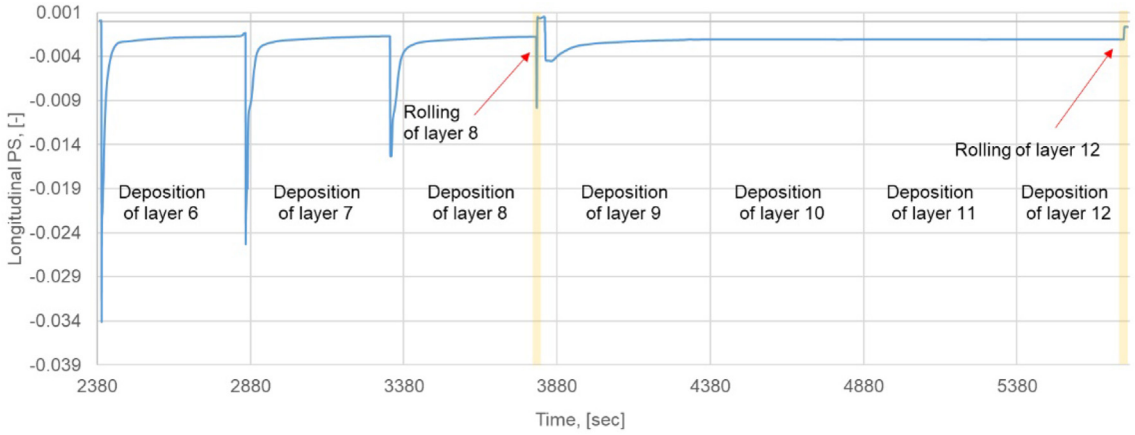

Fig. 18. Evolution of longitudinal PS in the layer 6 during WAAM deposition and stacked 4L rolling with flat roller. The rolling phases are highlighted in the yellow shaded areas. (For interpretation of the references to colour in this figure legend, the reader is referred to the web version of this article.)

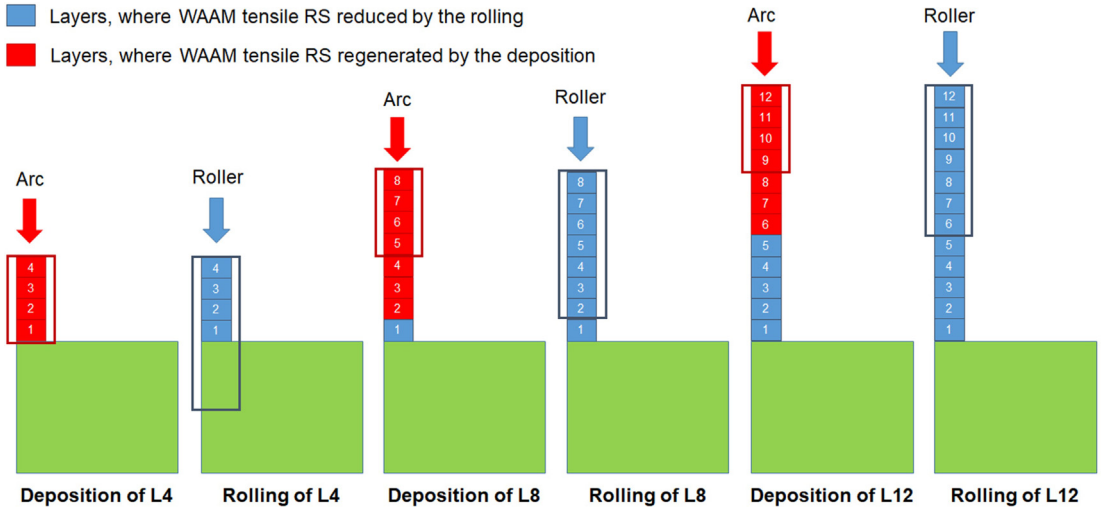

Fig. 19. Schematic of cyclic variation of longitudinal RS during WAAM + stacked 4L rolling with flat roller. The boxed red and blue layers are those influenced by WAAM deposition and rolling, respectively. (For interpretation of the references to colour in this figure legend, the reader is referred to the web version of this article.)

Based on the above evaluation considering the stress/distortion mitigation effectiveness, geometric control and manufacturing efficiency, the stacked 4L rolling with the slotted roller is potentially an optimal process for building straight wall components.

5. Conclusions

Efficient coupled process models for inter-layer rolling, stacked-layers rolling and post-build rolling were developed to investigate the residual stress and distortion mitigation by vertical rolling in a WAAM steel wall. The models were validated using previous experimental results. The concurrent evolution of temperature, plastic strain and residual stress during WAAM deposition and inter-layer rolling was revealed to understand the interaction between deposition and rolling. Optimisation of the rolling strategy for the hybrid process was also conducted to enhance manufacturing efficiency without compromising the stress/distortion mitigation efficacy. The following conclusions are drawn:

1. Changing the number of deposition layers for each rolling cycle and modifying the roller geometry leads to different influence depths of WAAM deposition and rolling. The process influence depth is manifested as the reaching depth of the plastic flow induced by the deposition or rolling of each layer. The greater the influence depth, the more extensive the effect of the process on the residual stress. The difference in influence depth affects the interaction between the deposition and rolling during the hybrid process, which governs the final residual stress and distortion in the WAAM-built component.
2. Cyclic re-formation of tensile residual stress occurs during WAAM deposition. The inter-layer rolling with the flat roller has smaller influence depth compared to the deposition. Therefore, the rolling mainly reduces the degree of the re-formation of the WAAM tensile residual stress during the consecutive deposition of layers. Thanks to the lateral restraint of the slot, the rolling with the slotted roller promotes more longitudinal tensile plastic deformation, despite its similar influence depth to the deposition. Consequently, the slotted roller reduces the tensile residual stress more significantly than the flat roller, and it also produces compressive residual stress more extensively.
3. Stacked-layers rolling can be used as an alternative to inter-layer rolling to reduce the manufacturing time. The stacked-four-layer rolling process is implemented with fewer rolling operations than the inter-layer rolling. Fortunately, it has larger influence depth than the deposition and thereby leads to longi-

tudinal residual stress distributions similar to those produced by the inter-layer rolling. The stacked-layers rolling with slotted roller is highly effective and has additional benefits such as marginal change of wall dimensions and low surface roughness, and hence it is potentially optimal for the hybrid process.
4. Post-build rolling has relatively large influence depth, but it is not as effective as the inter-layer and stacked-layers rolling to reduce the residual stress in the whole WAAM wall studied here, since the penetration is insufficient for a tall wall. Nevertheless, it could be efficiently applied to lower height WAAM components.
5. As the rolling mitigates the deposition-induced tensile residual stress in the clamped WAAM component, the distortion due to the tensile stress relaxation after removal of clamps is reduced by the rolling. The slotted roller is more effective than the flat roller in reducing distortion, since it can more significantly mitigate the WAAM residual stress.

CRediT authorship contribution statement

Valeriy Gornyakov: Conceptualization, Methodology, Software, Formal analysis, Investigation, Data curation, Writing – original draft, Visualization. **Yongle Sun:** Conceptualization, Formal analysis, Investigation, Resources, Writing – review & editing, Supervision. **Jialuo Ding:** Conceptualization, Resources, Writing – review & editing, Supervision, Project administration. **Stewart Williams:** Conceptualization, Resources, Supervision, Project administration.

Data availability

Data underlying this study can be accessed through the Cranfield University repository at https://doi.org/10.17862/cranfield.rd.19199765.

Declaration of Competing Interest

The authors declare that they have no known competing financial interests or personal relationships that could have appeared to influence the work reported in this paper.

Acknowledgements

Initial part of this research was guided and supported by Dr. Paul Colegrove. Part of this research was technically supported by Drs. Daniel Cozzolino, Filomeno Martina and Matyas Benke. The support by NEWAM programme (EPSRC grant EP/R027218/1) and WAAMMat is also acknowledged.

References

[1] Layer by layer Cost effective manufacturing of metal components Wire Arc Additive Manufacturing, (n.d.). <http://fronius.com.tw/en/welding-technology/info-centre/magazine/2019/waam> (Accessed February 23, 2021).
[2] Additive Manufacturing solutions. Vallourec have selected two technologies to improve the future of the metallic component value chain for the Oil & Gas market: Thermal spray and Wire Arc Additive Manufacturing (WAAM), (n.d.). <https://solutions.vallourec.com/en/Oil-and-Gas/OCTG/Products/Additive-Manufacturing> (Accessed February 23, 2021).
[3] J.M. Fletcher, The Future for WAAM, Additive Manufacturing AMazing. (n.d.). <http://additivemanufacturing.com/2019/08/27/the-future-for-waam/> (Accessed February 23, 2021).
[4] Y. Li, C. Su, J. Zhu, Comprehensive review of wire arc additive manufacturing: Hardware system, physical process, monitoring, property characterization, application and future prospects, Results Eng. 13 (2022) 100330, https://doi.org/10.1016/j.rineng.2021.100330.
[5] P.A. Colegrove, H.E. Coules, J. Fairman, F. Martina, T. Kashoob, H. Mamash, L.D. Cozzolino, Microstructure and residual stress improvement in wire and arc additively manufactured parts through high-pressure rolling, J. Mater. Process. Technol. 213 (2013) 1782–1791, https://doi.org/10.1016/j.jmatprotec.2013.04.012.
[6] T.A. Rodrigues, V.R. Duarte, D. Tomás, J.A. Avila, J.D. Escobar, E. Rossinyol, N. Schell, T.G. Santos, J.P. Oliveira, In-situ strengthening of a high strength low alloy steel during Wire and Arc Additive Manufacturing (WAAM), Addit. Manuf. 34 (2020) 101200, https://doi.org/10.1016/j.addma.2020.101200.
[7] B. Cong, X. Cai, Z. Qi, B. Qi, Y. Zhang, R. Zhang, W. Guo, Z. Zhou, Y. Yin, X. Bu, The effects of ultrasonic frequency pulsed arc on wire + arc additively manufactured high strength aluminum alloys, Addit. Manuf. 51 (2022) 102617, https://doi.org/10.1016/j.addma.2022.102617.
[8] M.M. Tawfik, M.M. Nemat-Alla, M.M. Dewidar, Enhancing the properties of aluminum alloys fabricated using wire + arc additive manufacturing technique – a review, J. Mater. Res. Technol. 13 (2021) 754–768, https://doi.org/10.1016/j.jmrt.2021.04.076.
[9] Z. Lin, K. Song, X. Yu, A review on wire and arc additive manufacturing of titanium alloy, J. Manuf. Process. 70 (2021) 24–45, https://doi.org/10.1016/j.jmapro.2021.08.018.
[10] C. Xiaolong, L. Zulei, G. Yanhua, S. Zhonggang, W. Yaoqi, Z. Lian, A study on the grain refinement mechanism of Ti-6Al-4V alloy produced by wire arc additive manufacturing using hydrogenation treatment processes, J. Alloy. Compd. 890 (2022) 161634, https://doi.org/10.1016/j.jallcom.2021.161634.
[11] G. Asala, A.K. Khan, J. Andersson, O.A. Ojo, Microstructural analyses of ATI 718Plus® produced by wire-ARC additive manufacturing process, Metall. Mat. Trans. A. 48 (2017) 4211–4228, https://doi.org/10.1007/s11661-017-4162-2.
[12] R.M. Kindermann, M.J. Roy, R. Morana, P.B. Prangnell, Process response of Inconel 718 to wire + arc additive manufacturing with cold metal transfer, Mater. Des. 195 (2020) 109031, https://doi.org/10.1016/j.matdes.2020.109031.
[13] C. Shen, Z. Pan, D. Cuiuri, J. Roberts, H. Li, Fabrication of Fe-FeAl functionally graded material using the wire-arc additive manufacturing process, Metall. Mater. Trans. B. 47 (2016) 763–772, https://doi.org/10.1007/s11663-015-0509-5.
[14] T.A. Rodrigues, N. Bairrão, F.W.C. Farias, A. Shamsolhodaei, J. Shen, N. Zhou, E. Maawad, N. Schell, T.G. Santos, J.P. Oliveira, Steel-copper functionally graded material produced by twin-wire and arc additive manufacturing (T-WAAM), Mater. Des. 213 (2022) 110270, https://doi.org/10.1016/j.matdes.2021.110270.
[15] D. Clark, M.R. Bache, M.T. Whittaker, Shaped metal deposition of a nickel alloy for aero engine applications, J. Mater. Process. Technol. 203 (2008) 439–448, https://doi.org/10.1016/j.jmatprotec.2007.10.051.
[16] S.R. Singh, P. Khanna, Wire arc additive manufacturing (WAAM): a new process to shape engineering materials, Mater. Today:. Proc. 44 (2021) 118–128, https://doi.org/10.1016/j.matpr.2020.08.030.
[17] P.J. Withers, H.K.D.H. Bhadeshia, Residual stress part 2 - Nature and origins, Mater. Sci. Technol. 17 (2001) 366–375.
[18] P. Dong, F.W. Brust, Welding residual stresses and effects on fracture in pressure vessel and piping components: a millennium review and beyond, J. Pressure Vess. Technol. 122 (2000) 329–338, https://doi.org/10.1115/1.556189.
[19] G.A. Webster, A.N. Ezeilo, Residual stress distributions and their influence on fatigue lifetimes, Int. J. Fatigue 23 (2001) 375–383, https://doi.org/10.1016/S0142-1123(01)00133-5.
[20] H.V. Cordiano, Effect of residual stresses on the low cycle fatigue life of large scale weldments in high strength steel, J. Eng. Ind. 92 (1970) 86–92, https://doi.org/10.1115/1.3427724.
[21] N. van den Berg, H. Xin, M. Veljkovic, Effects of residual stresses on fatigue crack propagation of an orthotropic steel bridge deck, Mater. Des. 198 (2021) 109294, https://doi.org/10.1016/j.matdes.2020.109294.
[22] X. Bai, H. Zhang, G. Wang, Modeling of the moving induction heating used as secondary heat source in weld-based additive manufacturing, Int. J. Adv. Manuf. Technol. 77 (2015) 717–727, https://doi.org/10.1007/s00170-014-6475-2.
[23] H. Shen, J. Lin, Z. Zhou, B. Liu, Effect of induction heat treatment on residual stress distribution of components fabricated by wire arc additive manufacturing, J. Manuf. Process. 75 (2022) 331–345, https://doi.org/10.1016/j.jmapro.2022.01.018.
[24] C. Shen, M. Reid, K.-D. Liss, Z. Pan, Y. Ma, D. Cuiuri, S. van Duin, H. Li, Neutron diffraction residual stress determinations in Fe3Al based iron aluminide components fabricated using wire-arc additive manufacturing (WAAM), Addit. Manuf. 29 (2019) 100774, https://doi.org/10.1016/j.addma.2019.06.025.
[25] X. Wang, A. Wang, Y. Li, A sequential path-planning methodology for wire and arc additive manufacturing based on a water-pouring rule, Int. J. Adv. Manuf. Technol. 103 (2019) 3813–3830, https://doi.org/10.1007/s00170-019-03706-1.
[26] F. Martina, M.J. Roy, B.A. Szost, S. Terzi, P.A. Colegrove, S.W. Williams, J. Meyer, M. Hofmann, Residual stress of as-deposited and rolled wire+arc additive manufacturing Ti–6Al–4V components, Mater. Sci. Technol. 32 (2016) 1439–1448, https://doi.org/10.1080/02670836.2016.1142704.
[27] J.R. Hönnige, P.A. Colegrove, B. Ahmad, M.E. Fitzpatrick, S. Ganguly, T.L. Lee, S. W. Williams, Residual stress and texture control in Ti-6Al-4V wire + arc additively manufactured intersections by stress relief and rolling, Mater. Des. 150 (2018) 193–205, https://doi.org/10.1016/j.matdes.2018.03.065.
[28] S.M. Hwang, S. Kobayashi, Preform design in plane-strain rolling by the finite-element method, Int. J. Mach. Tool Des. Res. 24 (1984) 253–266, https://doi.org/10.1016/0020-7357(84)90060-X.
[29] C.H. Lee, S. Kobayashi, New solutions to rigid-plastic deformation problems using a matrix method, J. Eng. Ind. 95 (1973) 865–873, https://doi.org/10.1115/1.3438238.

[30] L.D. Cozzolino, H.E. Coules, P.A. Colegrove, S. Wen, Investigation of post-weld rolling methods to reduce residual stress and distortion, J. Mater. Process. Technol. 247 (2017) 243–256, https://doi.org/10.1016/j.jmatprotec.2017.04.018.
[31] V. Gornyakov, Y. Sun, J. Ding, S. Williams, Computationally efficient models of high pressure rolling for wire arc additively manufactured components, Appl. Sci. 11 (2021) 402, https://doi.org/10.3390/app11010402.
[32] V. Gornyakov, Y. Sun, J. Ding, S. Williams, Efficient determination and evaluation of steady-state thermal-mechanical variables generated by wire arc additive manufacturing and high pressure rolling, Model. Simul. Mater. Sci. Eng. (2021). https://doi.org/10.1088/1361-651X/ac35b8.
[33] V. Gornyakov, J. Ding, Y. Sun, S. Williams, Understanding and designing post-build rolling for mitigation of residual stress and distortion in wire arc additively manufactured components, Mater. Des. 213 (2022) 110335, https://doi.org/10.1016/j.matdes.2021.110335.
[34] M. Abbaszadeh, J.R. Hönnige, F. Martina, L. Neto, N. Kashaev, P. Colegrove, S. Williams, B. Klusemann, Numerical investigation of the effect of rolling on the localized stress and strain induction for Wire + Arc Additive Manufactured structures, J. Mater. Eng. Perform. 28 (2019) 4931–4942, https://doi.org/10.1007/s11665-019-04249-y.
[35] R. Tangestani, G.H. Farrahi, M. Shishegar, B.P. Aghchehkandi, S. Ganguly, A. Mehmanparast, Effects of vertical and pinch rolling on residual stress distributions in wire and arc additively manufactured components, J. Mater. Eng. Perform. 29 (2020) 2073–2084, https://doi.org/10.1007/s11665-020-04767-0.
[36] J. Gu, J. Ding, S.W. Williams, H. Gu, P. Ma, Y. Zhai, The effect of inter-layer cold working and post-deposition heat treatment on porosity in additively manufactured aluminum alloys, J. Mater. Process. Technol. 230 (2016) 26–34, https://doi.org/10.1016/j.jmatprotec.2015.11.006.
[37] J. Goldak, A. Chakravarti, M. Bibby, A new finite element model for welding heat sources, Metall. Trans. B 15 (1984) 299–305, https://doi.org/10.1007/BF02667333.
[38] J. Ding, P. Colegrove, J. Mehnen, S. Ganguly, P.M. Sequeira Almeida, F. Wang, S. Williams, Thermo-mechanical analysis of Wire and Arc additive layer manufacturing process on large multi-layer parts, Comput. Mater. Sci. 50 (2011) 3315–3322, https://doi.org/10.1016/j.commatsci.2011.06.023.
[39] H.E. Coules, G.C.M. Horne, S. Kabra, P. Colegrove, D.J. Smith, Three-dimensional mapping of the residual stress field in a locally rolled aluminium alloy specimen, J. Manuf. Processes 26 (2017) 240–251, https://doi.org/10.1016/j.jmapro.2017.02.010.
[40] J. Perenda, J. Trajkovski, A. Žerovnik, I. Prebil, Residual stresses after deep rolling of a torsion bar made from high strength steel, J. Mater. Process. Technol. 218 (2015) 89–98, https://doi.org/10.1016/j.jmatprotec.2014.11.042.
[41] J. Lan, S. Feng, L. Hua, The residual stress of the cold rolled bearing race, Proc. Eng. 207 (2017) 1254–1259, https://doi.org/10.1016/j.proeng.2017.10.879.
[42] T.A. Stolarski, S. Tobe, Rolling Contacts, John Wiley & Sons, Ltd, Chichester, UK, 2000. <https://doi.org/10.1002/9781118903001>.
[43] Thompson M.A., Fresini M., DosSantos J., Hedgegard J., Richardson I.M., Improving the competitiveness of the European steel fabrication industry using synchronised tandem wire welding technology, SYNFAB, 2005.
[44] R.H. Leggatt, Residual stresses in welded structures, Int. J. Press. Vessels Pip. 85 (2008) 144–151, https://doi.org/10.1016/j.ijpvp.2007.10.004.
[45] The Neutron Diffraction (ND) technique measures residual stresses deep within a material by detecting the diffractions of an incident neutron beam., (n.d.). <https://www.veqter.co.uk/residual-stress-measurement/neutron-diffraction> (Accessed March 13, 2021).
[46] R.C. McCLUNG, A literature survey on the stability and significance of residual stresses during fatigue, Fat. Frac. Eng. Mat. Struct. 30 (2007) 173–205, https://doi.org/10.1111/j.1460-2695.2007.01102.x.
[47] S.M. Hassani-Gangaraj, M. Carboni, M. Guagliano, Finite element approach toward an advanced understanding of deep rolling induced residual stresses, and an application to railway axles, Mater. Des. 83 (2015) 689–703, https://doi.org/10.1016/j.matdes.2015.06.026.
[48] J. Donoghue, A.A. Antonysamy, F. Martina, P.A. Colegrove, S.W. Williams, P.B. Prangnell, The effectiveness of combining rolling deformation with Wire-Arc Additive Manufacture on β-grain refinement and texture modification in Ti–6Al–4V, Mater. Charact. 114 (2016) 103–114, https://doi.org/10.1016/j.matchar.2016.02.001.
[49] H.E. Coules, P. Colegrove, L.D. Cozzolino, S.W. Wen, S. Ganguly, T. Pirling, Effect of high pressure rolling on weld-induced residual stresses, Sci. Technol. Weld. Joining 17 (2012) 394–401, https://doi.org/10.1179/1362171812Y.0000000021.

2022-09-22

Modelling and optimising hybrid process of wire arc additive manufacturing and high-pressure rolling

Gornyakov, Valeriy

Elsevier

Gornyakov V, Sun Y, Ding J, Williams S. (2022) Modelling and optimising hybrid process of wire arc additive manufacturing and high-pressure rolling. Materials and Design, Volume 223, November 2022, Article number 111121

https://doi.org/10.1016/j.matdes.2022.111121